HEFAT2011
8th International Conference on Heat Transfer, Fluid Mechanics and Thermodynamics
11 – 13 July 2011
Pointe Aux Piments, Mauritius

HEAT TRANSFER ENHANCEMENT, FLOW VISUALIZATION AND FRICTION CHARACTERISTICS IN RIB-ROUGHENED CHANNELS

Stasiek A., Jewartowski M., Mikielewicz D. and Stasiek J.*
*Author for correspondence
Department of Energy and Industrial Apparatus,
Gdansk University of Technology,
80-233 Gdansk, Narutowicza 11/12
Poland,
E-mail: jstasiek@pg.gda.pl

ABSTRACT

In the last two decades thermochromic liquid crystal (TLS), true-color digital image processing and laser anemometry (PIV) have been successfully used in non-intrusive, technical and heat and mass transfer studies and applications. The aim of the paper is to asses the state of the art in the exploration of heat transfer control by transverse vortex generators. They are able to increase heat transfer by several hundred percent. Prior to the use of vortices to influence heat transfer it must be known how different vortices are generated and controlled and how they interact with the original or base flow and temperature field. Liquid crystals were used to determinate the distribution of surface temperature and then evaluation of heat transfer coefficient or the Nusselt number. The flow pattern produced by transverse vortex generators (rib-roughened passages) was visualized using a planar beam of double-impulse laser tailored by a cylindrical lens and oil particles. Sequential images of particles in the cross sectional plane taken with CCD video camera from the downstream side the flow were stored on a personal computer to obtain distributions of velocity vectors by means of the PIV method. Local and average Nusselt numbers, friction factors and velocity fields are presented for rectangular channels with an aspect ratio of 6.35 and five types of transverse vortex generators which were brought to required temperatures by hot film method. The pitch-to-height-ratio of the ribs was 11.

INTRODUCTION

Vortices and their generators incorporate three enhancement mechanisms (swirl, flow destabilization and developing viscous layers). Vortices swirl fluid around their axis of rotation, they induce velocity profiles which are less stable, and their generation implies flow separation and developing viscous layers [1,2]. Even though everybody knows what is meant by a vortex, namely swirling flow, an agreed upon mathematical definition of a vortex, very helpful for vortex identification, does not exist, even though vorticity $\nabla \times \varpi$, and also vortex line and vortex tube are well defined mathematically.

NOMENCLATURE

c	[J/kgK]	Specific heat
D_h	[m]	Hydraulic channel diameter
f	[-]	Equivalent friction coefficient
h	[W/m^{2}K]	Heat transfer coefficient
I	[A]	Electric current
k	[W/mK]	Thermal conductivity
l	[m]	Length
n	[-]	Number of measurements
Nu	[-]	Nusselt number
Pr	[-]	Prandtl number
q	[W/m^2]	Heat flux
r	[Ω]	Electrical resistance
Re	[-]	Reynolds number
t	[s]	Time
T	[K, deg]	Temperature
TI	[%]	Turbulence intensity
u	[m/s]	Velocity
X	[m]	Thickness
δ	[m]	Plate wall thickness
ΔP	[Pa]	Pressure lost
ρ	[kg/m^3]	Density

Subscripts

a	Air
av	Average
b	Water-side
i	Instantaneous
in	Initial
n	Local (net) surface
o	For smooth channel
w	Wall
α	Time-averaged

Such vortices do not only swirl but also destabilize the flow, which is well known for transverse vortices (TV), the Karman vortex street behind a cylinder in cross flow is probably the best

known example. The destabilization effects of longitudinal vortices (LV) are still under investigation. One of the reasons is that single LVs are more difficult to generate than TVs. Self-sustained oscillations associated with vortices have been exploited very little in general and specially for heat transfer purposes. The third mechanism, i.e. viscous layer interruption and initiation of new developing viscous layers is implied by vortex generation (VG) [3,4].

To use vortices to influence heat transfer it must be known how different vortices are generated and controlled and how they interact with the original or base flow and temperature field. Special attention will be given to the influence of geometrical VG variations on self-sustained oscillations, flow visualization and heat transfer.

METHODOLOGY AND EXPERIMENTAL SETUP

Liquid Crystal Thermography

Thermochromic liquid crystals (TLC) and true-colour digital image processing have been successfully used in nonintrusive technical, industrial and biomedical studies and applications [5]. Thin coatings of TLC's at surfaces are utilized to obtain detailed temperature distributions and heat transfer rates for steady or transient processes.

Liquid Crystals Themography (so called LCT) have been extensively applied to the qualitative visualization of the entire steady state, or transient temperature fields on solid surfaces. Since quantifying colour is a difficult and somewhat ambiguous task, application of thermochromic liquid crystals initially was largely qualitative. Application of the colour films or interference filters was tedious and inaccurate. The first application of true-colour digital image processing gave impact to qualitative and fast temperature measurements. Rapid development of image processing techniques has made it now possible to set-up inexpensive systems capable of real-time transient full field temperature measurements using TLCs. Before the execution of a thermal or flow visualization experiment, we should recognize the characteristics of the overall combination of the TLC, the light source, the optical and camera system, and make a rational plan for the total measurement system. The relationship between the temperature of the crystal and the measured Hue of the reflected light defines the calibration curve for the specified liquid crystal [5]. The distribution of the colour component pattern on the liquid crystal layer was measured by RGB colour camera and a series of images at different temperatures defines the calibration. Two main methods of surface temperature measurements could be performed involving steady state and transient techniques. A brief history of these is given by Baughn et al [4] and Stasiek [5].

The steady liquid crystal (LC) method allows the entire surface to be mapped from one LC image using a colour processing system. To overcome the problem of limited colour play range, the heat flux into the surface can be adjusted so as to move the colour band to different locations and thus progressively map the heat transfer coefficient over the entire test section. The transient LC method is based on the fact that when the test surface of a uniform initial temperature is suddenly exposed to a uniformly heated or cooled flow, the magnitudes of the time-varying surface temperature is governed by transient heat conduction penetrating into a seminfinite solid (see, for instance Ref [6]). In current study special attention was focused on local and average heat transfer coefficients (in Nusselt form) on the inter-rib regions of the heated plate. The experimental study was also performed by using the steady-state liquid crystal technique.

Steady State Analyses - Constant Flux Method:

The steady state techniques employ a heated model and the TLC is used to monitor the surface temperature T_w. It gives the local heat transfer coefficient:

$$h = \frac{q}{T_w - T_a} \tag{1}$$

where:

$$q = I^2 r \tag{2}$$

Steady State Analyses - Uniform Temperature Method:

The TLC-coated test specimen forms one side of a constant temperature water bath and is exposed to a cool/hot air flow. In this case, the heat transfer coefficient:

$$h = \frac{k_w}{x_w}\frac{\left(T_w - T_{w,b}\right)}{\left(T_a - T_w\right)} \tag{3}$$

Transient Method:

This technique requires measurement of the elapsed time to increase the surface temperature of the TLC coated test specimen from a known initial temperature predetermined value. Leiner et al [6], developed the formula for evaluation of heat transfer coefficient:

$$h = -\frac{\delta\rho c}{t} ln\left[\frac{T_{a,in} - T}{T_{a,in} - T_{w,in}}\right] \tag{4}$$

where the transient local surface temperature T is detected after a time interval t.

Image processing by digital computer

Problem of processing natural-quality imagery can be solved with the use of computers and appropriate software. Optical processes, communication systems, and automatic image detection are three areas in which computer techniques are being applied. Interesting areas of research are those involving image restoration and enhancement.

Data Translation Ltd. [7] is one of the recognized leaders in the design, manufacture, and marketing of high-performance data acquisition image-processing boards and software. Fig. 1 shows the system flow chart, with one branch for video recording and one for application, respectively. As shown, the chart is for an RGB camera and includes IBM Personal Computer, HSI Color Frame Grabber DT 2871, Auxiliary Frame Processor DT 2868, JVC BR-S605EB S-VHS Recorder, KM V7EK Converter, and VT 3000 TBC Cards.

The video output section of the DT 2871 incorporates a 10-MH/HSI/RGB converter for transforming HSI pixels back into

RGB pixels after processing HSI/RGB colour space conversion is performed at 30 frames/s for display on colour monitors. For speeding computer-intensive colour processing, the DT 2871 Colour Frame Grabber connects directly to a DT-Connect processor board, which is controlled by Global Lab colour software. This system (without BR-S605EB) was first used to reinterpret colour image records from the early experiments of Stasiek et al. [8,9] using cholesteric liquid crystals for the steady state techniques. For non-steady processes or transient conditions, the temporal history of the temperature or velocity field can be used to determine the local heat transfer coefficient and velocity distribution. The rate of heating or cooling, the colour change patterns, or velocity streams are recorded by JVC BR-S605EB video recorder. Installing a computer-controlled video system with JVC KMV7EK RGB converter and VT3000 TBC Cards new chart with JVC-S605EB as the terminal makes it possible for presentation tapes to be loaded, cued, and played exactly on schedule with all operations handled by the computer. This can even be done with unattended presentation via a modem. For a fast and transient method, accurate location of specific scenes or edit points JVC BR-S605EB is provided with a convenient, easy-to-use search dial. A time base corrector (TBC) controls times tracking systems and easy identification colour-coded images.

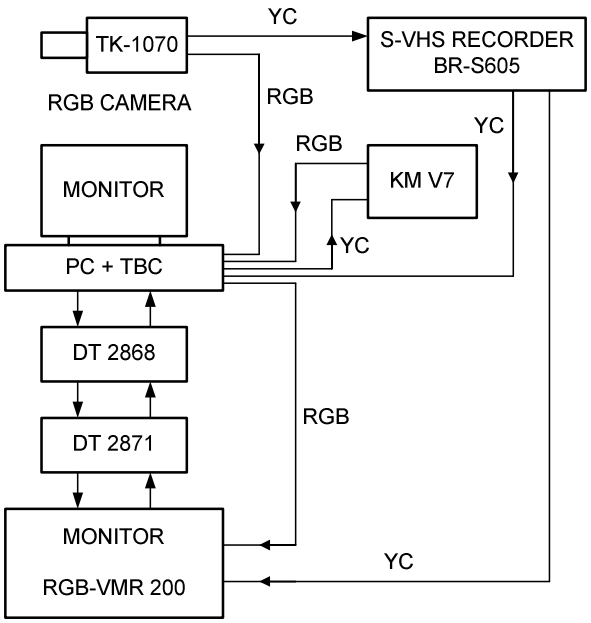

Figure 1 The information flow chart for a true colour image interpreter and computer-controlled video system

Open low speed wind-tunnel

The experimental study was carried out using an open low-speed wind tunnel consisting of entrance section with fan and heaters, large settling chambers with diffusing screen and honeycomb, and then working sections Fig. 2.

Air is drawn through the tunnel using a fan able to attain the Reynolds numbers in the range from 500 to 40 000. The working air temperature in the rig ranges from 15°C to 65°C produced by the heater or cooler positioned just downstream of the inlet. The major construction material of the wind tunnel is perspex. Local and mean velocity are measured using conventional Pitot tubes and DISA hot-wire velocity probe.

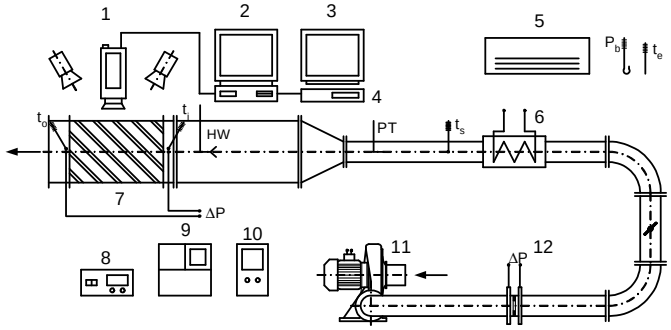

Figure 2 Open low speed wind-tunnel, 1 – RGB camera (TK-1070), 2 – PC, 3 – monitor (RGB-VMR 200), 4 – S-VHS recorder, 5 – air conditioning system, 6 – heater, 7 – LC mapping section, 8 – digital micro manometer FCO 12, 9 – DISA hot wire system, 10 – variac, 11 – fan, 12 – orifice.

The alternative effects of constant wall temperature and constant heat flux boundary conditions are obtained using plate electric heater [10]. Photographs are taken using RGB video-camera and a true-colour image processing technique.

The liquid crystals used here, manufactured in sheet form by Merck Ltd [11], had an event temperature range from 30.0 to 35.0 ^{o}C. In this particular experiment uncertainty for temperature measurement was estimated as about ± 0,05 ^{o}C by considering only the section of the surface used in the experiment, span-wise non-uniformities in Hue value are minimized.

In many cases, as mentioned above, remarkable enhancement of local and spatially averaged surface heat transfer rates are possible with rib turbulators, in spite of the lower local Nusselt number at certain locations along the ribbed surfaces. Prior to ribbed turbulator test section is a 255x40 mm inlet duct that is 550 mm in length. This is equivalent to 7,96 hydraulic diameter (where the hydraulic diameter is 69,11 mm).

Liquid Crystal Thermography and Particle Image Velocimetry measurements were performed in a flat transparent test section with unique rib-corrugation of the walls (Fig. 2). Ribs were a square 6 mm rods, placed on the top or bottom (or both) test section wall. In all cases distances between ribs were 66 mm (distance between centres of the neighbour ribs, measured in the flow direction). That led to the pitch-to-height-ratio of 11. Here we consider five different configurations of the wall corrugation (Fig. 3):

- first configuration: ribbed bottom wall only by 6 ribs placed perpendicularly to the flow direction (geometry a),
- second configuration: ribbed top and bottom walls, each by 6 ribs placed perpendicularly to the flow direction (geom. b),
- third configuration: robbed bottom wall only by 6 ribs inclined at 45° to the flow direction (geom. c),
- fourth configuration: ribbed top and bottom walls, 6 ribs on each wall, ribs parallel to each other and inclined at 45° to the flow direction (geom. d),

- fifth configuration: ribbed top and bottom walls, 6 ribs on each wall, ribs perpendicular to each other an inclined at 45° to the flow direction (geom. e).

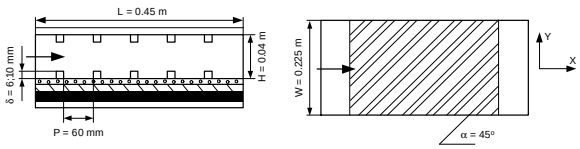

Figure 3 Schematic diagram of the rib turbulator test surfaces

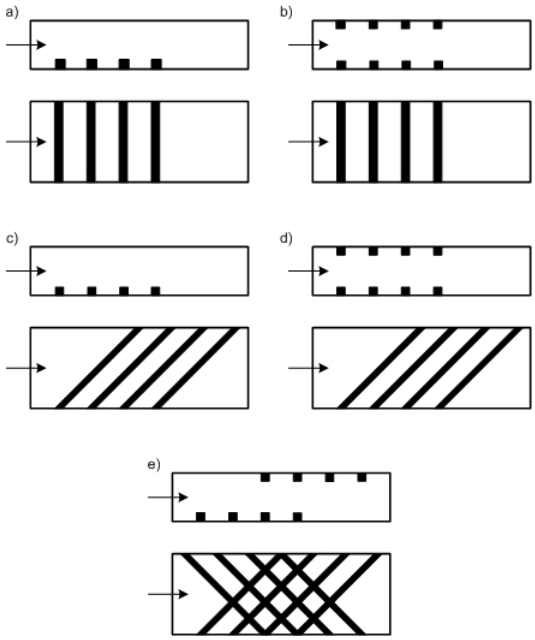

Figure 4 Five types of transverse vortex generators (cross-corrugated and rectangular ribs)

Particle Image Velocimetry (PIV)

Particle Image Velocimetry technique is a well-established experimental method in fluid mechanics, that allows quantitative measurement of two-dimensional flow structure. It enables the measurement of the instantaneous in-plane velocity vector field within a planar section of the flow field and allows to calculate spatial gradients, dissipation of turbulent energy, spatial correlations, and the like [12,13]. In PIV technique selected cross-section of the investigated seeded flow is illuminated by laser light formed in thin "light sheet" (Fig.5). Images of the flow are recorded by CCD camera and correlated to calculate instantaneous velocity fields.

The main part of the experimental set-up (Fig. 5) consists of a transparent model of ribbed channel, laser light source (30 mJ double pulse Nd:YAG laser *SoloPIV, New Wave Research, Inc.*) and high resolution 12bit digital CCD camera (1280 × 1024 pixels, *PCO SensiCam*). This system permits acquisition of two images at the minimum time interval of 200ns, exposition time of 5ns, and about 3.75Hz repetition rate. The PIV recording system installed on 3GHz Pentium 4 computer with 3GB RAM capable for acquisition over 200 pairs of images during a single experimental run.

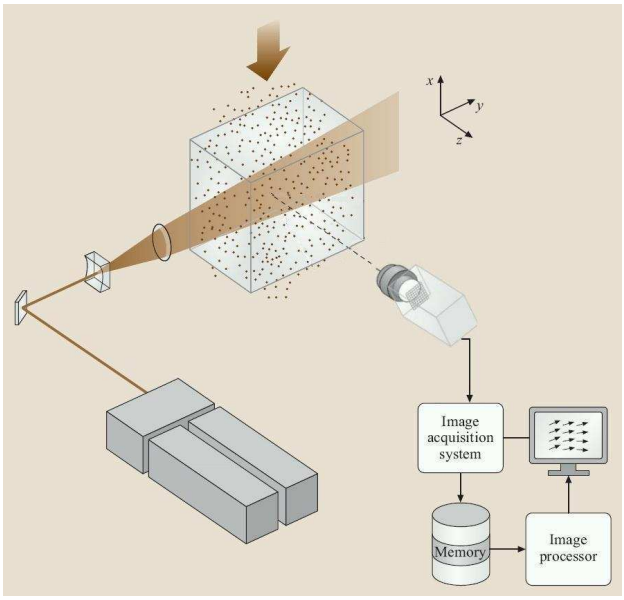

Figure 5 Schematic of a typical PIV measurement system

The PIV measurements were performed for pure air seeded with small droplets (few micrometers in diameter) of synthetic oil DEHS (Di-Ethyl-Heksyl-Sebacat). The oil drops volumetric concentration was very low (< 0.001), hence they did not affect the flow structure.

As results, 15 sets of velocity fields were obtained from the PIV measurements: for different ribs geometries and different Reynolds numbers (Re = 9000, 16000 and 26000). The area interrogated by the PIV method was in all cases located in the mid-vertical-plane between side walls.

EXPERIMENTAL RESULTS AND DISCUSSIONS

The heat transfer coefficient and the pressure drop per unit length are two of the most relevant parameters in the heat exchangers. This chapter presents measurement results of both parameters as well as velocity field obtained on model heat exchanger.

Experimental results - LCT

In the discussion that follows, the Nusselt number

$$Nu = h \cdot \frac{D_h}{k_a} \tag{5}$$

The heat transfer coefficient is then based on the flat projected area and is determined using

$$h = \frac{q_n}{\left(T_w - T_{a,\alpha}\right)} \tag{6}$$

where local surface temperature T_w is found from LCT, and T_α is the time – averaged, local mixed mean air temperature.

The surface Nusselt number distribution along the rib turbulator test surface for four Reynolds number are presented in Fig 6. for geometry c, while in Fig. 7 for geometry d. It is the evidence that transverse vortex generators (TVG_s) enhance heat

transfer by several hundred percent but only for certain Reylonds numbers. Comparison between the maps of velocity vectors and local Nusselt numbers contours reveals that high velocity do not enhance heat transfer in some cases, probably the moving fluid (with high velocity) does not penetrates into the boundary layer and flows above the ribs. Optimum flow condition should be established for high efficient enhancement of heat transfer augmentation in particular environment e.g. flow and heat exchanger configuration.

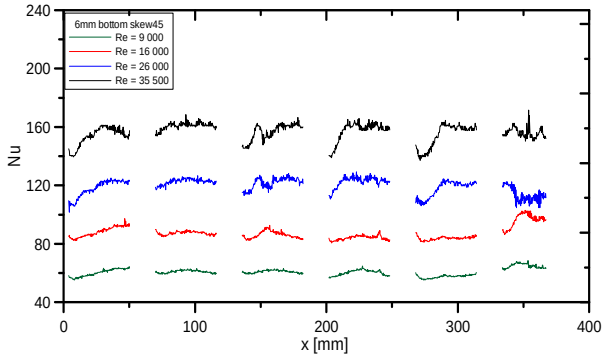

Figure 6 Nusselt number distribution in consecutive test sections for geometry c (Re=9000, 16000, 26000 and 35500)

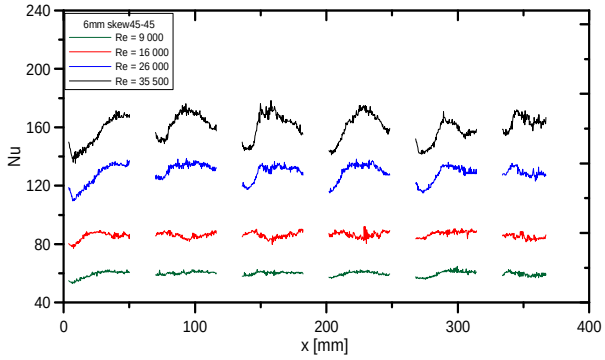

Figure 7 Nusselt number distribution in consecutive test sections for geometry d (Re=9000, 16000, 26000 and 35500)

Table 1 presents average Nusselt number distribution as well as average heat transfer coefficient taken between 3rd and 4th rib for each geometry.

For the purpose of comparison, calculations for the baseline condition of a smooth channel (without ribs) with asymetric heating were performed. The local Nusselt number was normalized by the Nusselt number for fully developed turbulent flow in smooth circular tubes Nu_o given by the well known Dittus-Boelter correlation:

$$Nu_o = 0.023 \cdot \mathrm{Re}^{0.8} \cdot \mathrm{Pr}^{0.4} \qquad (7)$$

Nusselt number Nu_o for smooth channel calculated according to Eq. (7) for given Reynolds numbers e.g. 9000, 16000, 26000 and 35500 results in the following data respectively: 29, 46, 68 and 87. Normalized Nusselt number Nu/Nu_o is presented in Fig. 8 as a function of the Reynolds number for all five ribs configurations. It was used to evaluate the performance of the rib-roughened channel. The best performance is given by geometry b, that is with ribbed bottom and top walls, perpendicular to the flow.

Table 1 Average Nusselt number and heat transfer coefficient distribution for different ribs geometry

Geometry	Re	h_{av}	Nu_{av}
a ribbed botom wall, perpendicular	9000	21,78	58,11
	16000	35,62	95,05
	26000	47,94	127,91
	35500	60,90	162,48
b ribbed bottom and top walls, perpendicular	9000	31,71	84,60
	16000	45,97	122,65
	26000	63,00	168,10
	35500	77,88	207,78
c ribbed bottom wall, inclined at 45°	9000	22,57	60,21
	16000	31,50	84,05
	26000	32,71	122,61
	35500	58,94	157,25
d ribbed bottom and top walls, inclined at 45°	9000	22,42	59,82
	16000	32,47	86,64
	26000	48,70	129,93
	35500	60,54	161,53
e ribbed bottom and top walls, inclined at 45° “grating”	9000	22,79	60,80
	16000	31,11	83,00
	26000	47,20	125,87
	35500	58,35	155,67

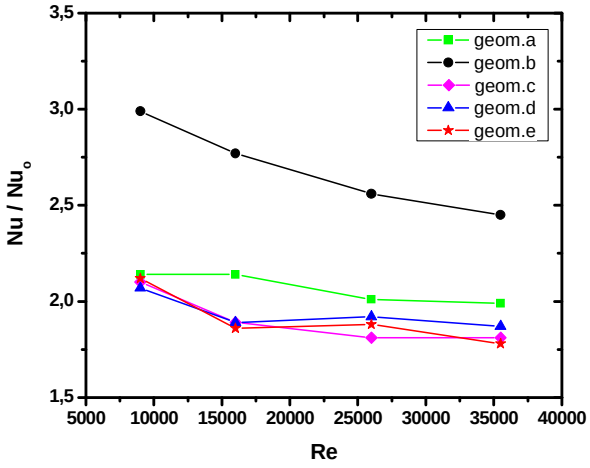

Figure 8 Normalized Nusselt number as a function of Reynolds number for different ribs geometry

Experimental results - PIV

Velocity fields were obtained from the PIV measurements for different ribs geometries and different Reynolds numbers (Re = 9000, 16000 and 26000). The area interrogated by the PIV method was in all cases located in the mid-vertical-plane between side walls.

Fig. 9a shows the average velocity field (averaged over 100 instantaneous velocity fields) for geometry c (with ribbed bottom wall inclined at 45°) ribs and Reynolds number Re = 26000. Maximum velocity for this case is about 7 m/s and is located in the upper part of the channel.

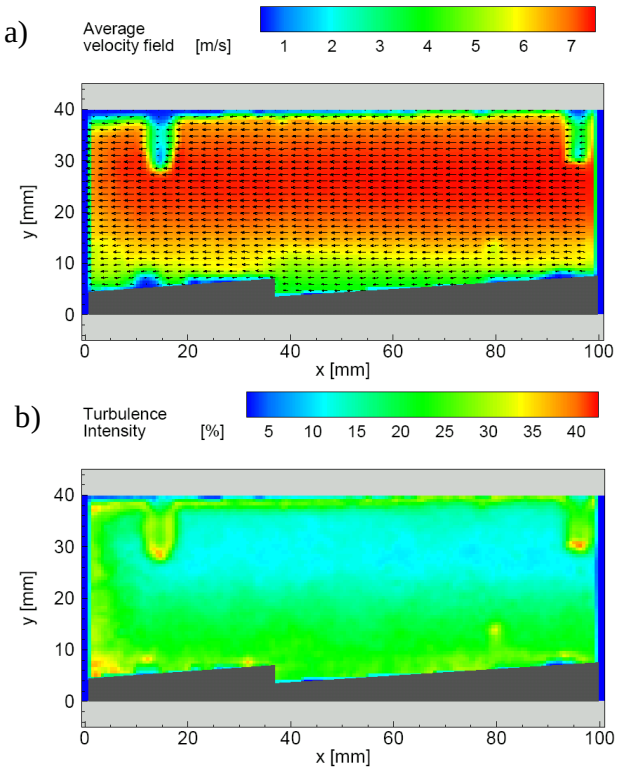

Figure 9 Averaged velocity field (a) and turbulence intensity (b) for geometry c and Reynolds number Re = 26000

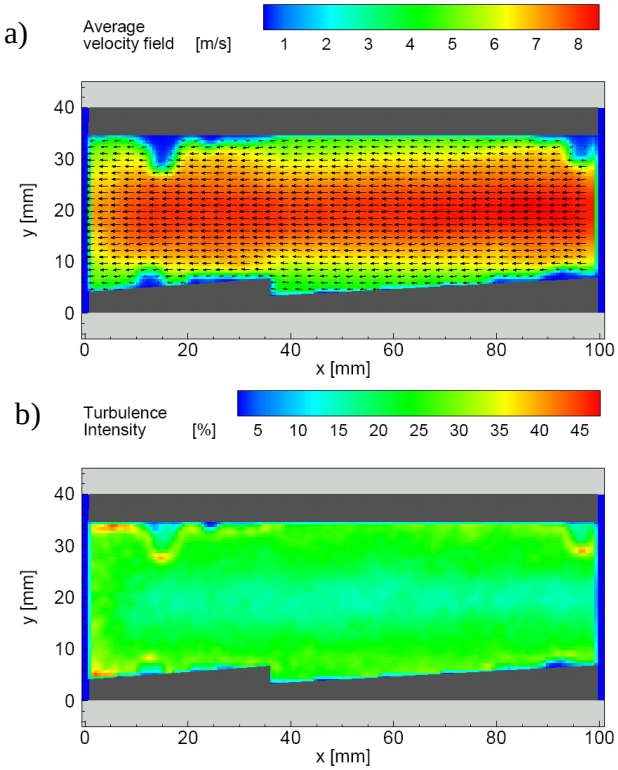

Figure 10 Averaged velocity field (a) and turbulence intensity (b) for geometry d and Reynolds number Re = 26000

Computed from 100 instantaneous velocity fields turbulence intensity (Fig. 9b), defined as:

$$TI = \frac{\left(\frac{1}{n}\sum_{i=1}^{n}(u_i - u_{av})^2\right)^{\frac{1}{2}}}{u_{av}} \cdot 100\% \qquad (8)$$

shows that flow is turbulent with maximum turbulence intensity of about 40% and decreases to 10% in top part of channel.

Fig. 10 presents the results for geometry d (ribbed bottom and top walls, inclined at 45º) but for the same Reynolds number Re=26000. Maximum velocity for this case is about 8 m/s and is located in the middle part of the channel. Turbulence intensity achieves maximum about 45% and is the smallest, around 12%, in the middle part of channel.

Pressure drop

The behaviour of equivalent friction coefficient f as a function of the Reynolds number for all five ribs configurations is presented in Fig. 11. Coefficient f was calculated for measured pressure drop from Darcy's formula [14]:

$$f = \frac{2 \cdot \Delta P \cdot D_h}{\rho \cdot u^2 \cdot l} \qquad (9)$$

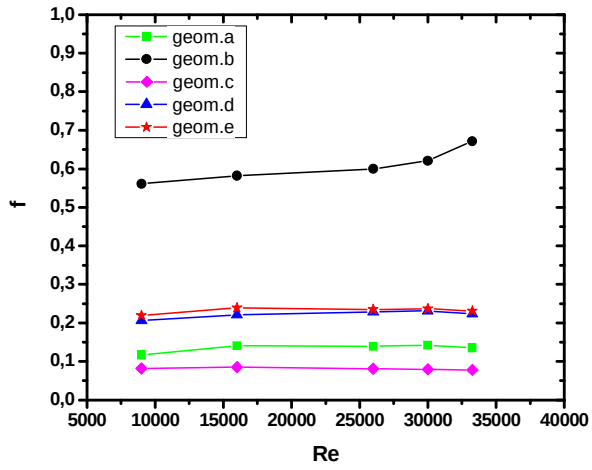

Figure 10 Equivalent friction coefficient f as a function of Reynolds number for different ribs geometry

High pressure drop corresponds to high Nusselt numbers. The biggest pressure drop as well as the highest average Nusselt number is for the geometry with ribbed bottom and top walls and perpendicular flow to the ribs (geometry b). Ribs inclined at 45º provide lower Nusselt numbers and lower pressure drop. The lowest pressure drop occurs for model with ribbed bottom wall inclined at 45º (geometry c).

CONCLUSION

A new experimental technique, in this case true-colour image processing of liquid crystal pattern and particle image velocimetry allows new approaches to old problems and the same time opens up new areas of research. Image processed

data makes available quantitative, full-field information about the distribution of temperature, flow visualization and heat transfer coefficient, which will undoubtedly encourage the study of situation which has been, until now, too complex to consider.

Heat transfer characteristics of rectangular channels with different ribs have been experimentally investigated by means of steady-state liquid crystal thermography. The corresponding average Nusselt number of the rib-roughened passages is generally two to three times higher in comparison to the smooth channel so heat transfer performance is better. Correlation of the flow velocity and heat transfer measurements elucidated mechanism limiting heat transfer coefficient for high flow rates. Future work will involve applying the present methods to more complex geometry and unsteady flow.

ACKNOWLEDGMENT

The work reported in this paper includes scientific cooperation between Gdansk University of Technology, Gdansk, Poland and Center of Mechanics, IPPT PAN, Warszawa, Poland. The financial assistance of Ministry of Science and Higher Education, Poland, Grant No. 3T10B07329 is kindly acknowledged.

REFERENCES

[1] Fiebig M., Vortices: Tools to Influence Heat Transfer – Recent Developments, *Proc. 2nd European Thermal Sciences and 14th UIT National Heat Transfer Conference*, 1996, pp 41-56

[2] Fiebig M., Vortex Generators for Compact Heat Exchangers, *J. of Enhanced Transfer* Vol.2, 1995, pp 43-61

[3] Moffat R.J., Experimental Heat Transfer *Proc. The Ninth International Heat Transfer Conference*, Jerusalem, Israel, 1990, pp 187-205

[4] Baughn J.W. and Yan X., Liquid Crystal Methods in Experimental Heat Transfer. *Proc. 32nd Heat Transfer and Fluid. California: Mechanics Institute Sacramento*, 1991, pp 15-40

[5] Stasiek J., Stasiek A., Jewartowski M. and Collins M.W., Liquid Crystal Thermography and True-Colour Digital Image Processing. *Optics & Laser Technology*, Vol. 38, 2006, pp 243-256

[6] Leiner W., Schulz K., Behle M., Lorenz S., Imaging techniques to measure local heat and mass transfer. *Proc. 3rd IMechE seminar Optical methods and data processing in heat and fluid flow*. City University, London, 1996, pp1-13

[7] DATA TRANSLATION Ltd.: Image Processing Handbook, 1991

[8] Stasiek J., Collins m.W., The use of liquid crystals and true-colour image processing in heat and fluid flow experiments, Atlas of Visualization, Vol.2, CRC Press, Inc. U.S.A. (1996)

[9] Stasiek J., Tanda G., Ciofalo M., Heat transfer measurement in heat exchangers by liquid crystal thermography, EUROMECH 406 COLLOQUIUM, Book of Abstracts IPPT PAN, Warsaw, Poland, May 6-8, (1999)

[10] MINCO Products, Inc., Minnesota, USA

[11] MERCK Ltd. Thermochromic Liquid Crystals. Broom Road, Poole, U.K.

[12] Kowalewski T.A., Ligrani P., Dreizler A., Schultz C. and Fey U. in C. Tropea, J. Foss and A. Yarin (ed.), Handbook of Experimental Fluid Mechanic, Chap. 7, Springer-Verlag, Berlin, Heidelberg 2007

[13] Raffel M., Willert C., Kompenhans J., Particle Image Velocimetry, A Practical Guide, Springer-Verlag, Berlin, 1998

[14] Massey B., Mechanics of Fluids, Revised by J.Ward-Smith, Stanley Thornes (Publishers) Ltd., United Kingdom, 1989